ELSEVIER

# An Investigation of the Constant-Temperature Hot-Wire Anemometer

**Jonathan H. Watmuff**
*MCAT Institute, NASA Ames Research Center, Moffett Field, California 94086*

■ An algorithm is developed for deriving the transfer functions of the constant-temperature hot-wire anemometer of arbitrary complexity. The only restriction is that the bridge elements, including the hot-wire filament, must be modeled by lumped components. A minimum of two equivalent amplifiers are required to model the feedback amplifier properly. The poles of the transfer functions for electronic and velocity perturbations are shown to be identical regardless of the frequency response characteristics of the feedback amplifier and the nature and quantity of components used to model the bridge impedances. Computer simulations are used to explore the behavior of representative configurations. It is shown that the frequency response characteristics of the feedback amplifier must be included in addition to the offset voltage and cable and balance inductance to fully account for the behaviour observed in real systems. This leads to an optimum system response when the balance inductor is in excess of that required for ac bridge balance. Increasing the frequency response and gain of the feedback amplifier have the rather surprising effect of increasing the damping of the dominant poles. It is the higher order poles that are responsible for the instabilities under these conditions. With subminiature wires it is shown that insufficient frequency response of the feedback amplifier is the most likely cause of instabilities. Operating modes are demonstrated that are misleading, in the sense that the operator can be deceived into interpreting an erroneous frequency response. Examples are provided to help operators of the instrument to identify and avoid these rather subtle and undesirable modes of operation. A brief description is given of a new high-performance anemometer design that is based on these considerations.

**Keywords:** *hot-wire, anemometer, instability, frequency response, transfer function*

## INTRODUCTION

Despite the shortcomings of the constant-temperature hot-wire anemometer it is still the most widely used means of measuring velocity fluctuations. In many situations, the behavior of the instrument can be explained using third-order models of the system behavior (e.g., [1, 2]). However, there are many aspects of the behavior of the instrument that cannot be accounted for in terms of existing theories. For example, instabilities are often encountered when using subminiature (e.g., $d = 0.5$ $\mu$m diameter) hot wires. Attempts to increase the overall frequency response by increasing the gain and frequency response of the feedback amplifier are invariably frustrated because the system develops instabilities.

The analysis reported in this paper was initially motivated by observations of hot-wire behavior in supersonic flow at the Gas Dynamics Laboratory at Princeton University. A frequency response requirement of 500 kHz is not uncommon in high-speed flows. Yet with extremely careful tuning of the system controls, by the most highly skilled operators and under the most favorable of circumstances, a barely adequate frequency response of around 250 kHz can be obtained with commercially available equipment. However, the phenomenon known as strain-gauging (in the form of small-amplitude high-frequency oscillations) was responsible for contamination of about three out of every four experimental runs (A. Smits, private communication). Sometimes the oscillations could

Address correspondence to Dr. Jonathan H. Watmuff, MCAT Institute, NASA Ames Research Center, Mail Stop 260-1, Moffett Field, CA 94035.

*Experimental Thermal and Fluid Science* 1995; 11:117–134

655 Avenue of the Americas, New York, NY 10010

0894-1777/95/$9.50
SSDI 0894-1777(94)00137-W

be made to disappear by adjusting the anemometer controls. This observation led me to propose that strain-gauging could be a purely electronic, rather than electromechanical, phenomenon and that a more sophisticated model of the system behavior could lead to further understanding and possible control of this frustrating problem.

It appears that the behavior of the constant-temperature hot-wire anemometer is not sufficiently well understood. A more complete understanding could lead to ways of avoiding instabilities and extending the frequency response. My original analysis [3] has been completely generalized and is presented here along with examples that will guide those who wish to build their own instruments and those who require the highest possible performance.

## MODEL OF THE CONSTANT-TEMPERATURE HOT-WIRE ANEMOMETER

It will be shown by example that the feedback amplifier must have the potential for both a high gain and a high-frequency response in order for the system as a whole to achieve stable high-frequency operation. Practical constant-temperature hot-wire anemometer designs should use a cascade of amplifiers rather than a single feedback amplifier because of the gain–bandwidth product limitations of physical devices. Therefore a cascade of $n$ amplifiers is used in the model shown in Fig. 1. The device labeled $I$ is a current booster stage that usually consists of a pair of power transistors. It will be assumed that the current booster has unity gain and zero offset exactly. The assumption of a perfect voltage follower means that the current booster need not be considered in the analysis. The behavior of each amplifier will be assumed to be linear with zero offset voltage. The net offset voltage of the amplifier cascade is controlled by introducing a dc voltage $E_{qi}$ and a perturbation voltage $e_S$ into the $m$th amplifier. The dc voltage is used to adjust the frequency response and stability of the system while the perturbation voltage is used for estimating the system frequency response. The perturbation voltage usually consists of a square wave, although sinusoidal inputs are sometimes used. In general, uppercase letters refer to dc quantities and lowercase letters refer to small perturbations. $Z_a(s)$, $Z_b(s)$, $Z_c(s)$, and $Z_w(s)$ represent the electrical impedances of each arm of the bridge, and $s$ is the Laplace variable.

## THE STATIC OPERATING POINT

Only the resistive components of the Wheatstone bridge need to be considered for the static (dc) analysis, that is, $Z_a(s) = R_a$, $Z_b(s) = R_b$, $Z_c(s) = R_c$, and $Z_w(s) = R_w$. The voltage at the top of the bridge, that is, the output of the $n$th amplifier, is given by

$$E_{o_n} = K_b\left[K_a(I_1R_a - I_2R_c) + E_{qi}\right] \tag{1}$$

where $K_a = K_1 \ldots K_{m-1}$ is the total gain of the cascade up to (but not including) the $m$th amplifier where the offset voltage is injected and $K_b = K_m \ldots K_n$ is the total gain of the cascade from the $m$th to the $n$th amplifier. The bridge voltage can also be expressed in terms of the currents $I_1$ and $I_2$,

$$E_{o_n} = I_1(R_a + R_w) \tag{2}$$

and

$$E_{o_n} = I_2(R_b + R_c). \tag{3}$$

Equations (1)–(3) lead to the following expression for the wire current:

$$I_1 = \frac{K_bE_{qi}(R_b + R_c)}{(R_a + R_w)(R_b + R_c) + K\mathring{R}}, \tag{4}$$

where $\mathring{R} = R_wR_c - R_aR_b$ represents the bridge imbalance and $K = K_aK_b$ is the overall gain of the cascade. Equation (4) represents the behaviour of the circuit.

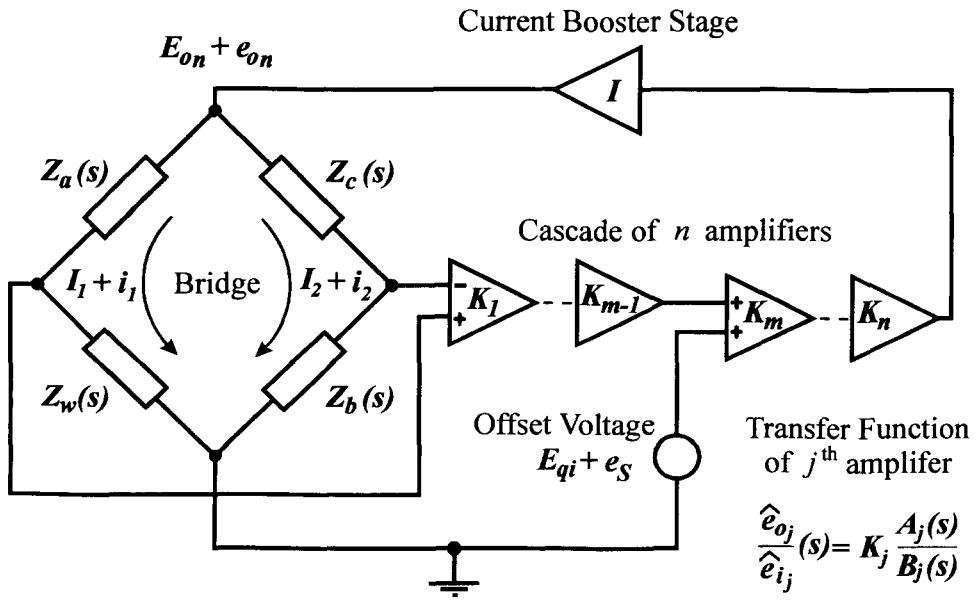


**Figure 1.** Model of constant-temperature hot-wire anemometer.

Following Smits et al. [4], an equation that represents the balance between the heat transfer and the Joule heating of the filament is given by

$$I_1^2 = \left(\frac{1}{R_g} - \frac{1}{R_w}\right)\frac{\pi l K_g \,\mathrm{Nu}}{c} \tag{5}$$

where $R_g$ is the wire resistance at gas temperature, $l$ is the length of the wire, $K_g$ is the thermal conductivity of the fluid, Nu is the Nusselt number, and $c$ is the temperature coefficient of resistivity of the wire material. The operating point is defined by the intersection of (4) with (5), which must be solved by iteration.

A number of important asymptotes and limits were identified by Perry and Morrison [2] with respect to the circuit equation. For example, the right-hand side of Eq. (4) must be indeterminate if $I_1$ is to remain finite as $E_{qi} \to 0$, that is,

$$(R_a + R_{wa})(R_b + R_c) + K\mathring{R}_a = 0, \tag{6}$$

where $\mathring{R}_a = R_{wa}R_c - R_aR_b$ is the value of $\mathring{R}$ corresponding to the asymptotic value of the wire resistance

$$R_{wa} = \frac{KR_aR_b - R_a(R_b + R_c)}{KR_c + (R_b + R_c)}. \tag{7}$$

They showed that perfect bridge balance can be achieved only in the limit as the offset voltage $E_{qi} \to 0$ and as the overall gain of the amplifier cascade $K \to \infty$. However, the quantity $K\mathring{R}$ always remains finite, even as the limits mentioned above are approached. The quantity $K\mathring{R}$ has a strong effect on the system stability and frequency response, and it is controlled by adjusting the offset voltage.

## TRANSFER FUNCTIONS FOR DYNAMIC RESPONSE

The circuit shown in Fig. 1 will be analyzed using Laplace transform methods as that lets us examine transient phenomena (such as the square-wave response) in addition to the usual steady-state sinusoidal response. It will be assumed that the dynamic behavior of any $j$th amplifier in the cascade can be adequately described by

$$\frac{\hat{e}_{o_j}}{\hat{e}_{i_j}}(s) = K_j\frac{A_j(s)}{B_j(s)}, \tag{8}$$

which is the transfer function for output voltage fluctuations in terms of the input voltage fluctuations. The circumflex denotes the Laplace transform, $K_j$ is the amplifier gain, and the roots of the polynomials $A_j(s)$ and $B_j(s)$ are the zeros and poles of the amplifier. From now on the circumflex will be dropped, but the Laplace transform is still implied.

In a physical circuit the current booster stage usually has a frequency response well in excess of that of the amplifiers. For the purpose of modeling it will be assumed that the frequency response is infinite in addition to the assumptions of exact unity gain and zero offset voltage. The assumption of an "ideal" current booster stage means that it need not be considered in the following analysis.

The small perturbation output voltage of the first amplifier in the cascade is given by

$$e_{o_1} = K_1\frac{A_1(s)}{B_1(s)}[i_1Z_a(s) - i_2Z_c(s)], \tag{9}$$

where $i_1$ and $i_2$ are the small perturbation bridge currents that are dependent on both offset voltage and velocity perturbations. The system transfer functions will be derived for these two cases.

### System Transfer Function for Offset Voltage Perturbations

In the absence of velocity fluctuations, the small perturbation currents $i_1$ and $i_2$ can be expressed in terms of the voltage fluctuation at the top of the bridge, that is, the output $e_{o_n}$ of the last ($n$th) amplifier,

$$i_1 = \frac{e_{o_n}}{Z_a(s) + Z_w(s)} \tag{10}$$

and

$$i_2 = \frac{e_{o_n}}{Z_b(s) + Z_c(s)}. \tag{11}$$

The electrical impedance of each arm of the bridge can be expressed as a transfer function relating voltage and current perturbations:

$$\begin{aligned} Z_a(s) &= \frac{Z_{a_N}(s)}{Z_{a_D}(s)}, \qquad Z_b(s) = \frac{Z_{b_N}(s)}{Z_{b_D}(s)}, \\ Z_c(s) &= \frac{Z_{c_N}(s)}{Z_{c_D}(s)}, \qquad \text{and} \qquad Z_w(s) = \frac{Z_{w_N}(s)}{Z_{w_D}(s)}. \end{aligned} \tag{12}$$

This representation is completely general, and an arbitrarily large number of elements can be used. The only restriction is that the elements must consist of lumped components. Using (10) and (11) to substitute for $i_1$ and $i_2$ in Eq. (9) and then applying Eq. (8) along the amplifier cascade leads to the expression for the output of the last ($n$th) amplifier $e_{o_n}$, that is,

$$\begin{aligned} e_{o_n} = {} & K_m \cdots K_n\frac{A_m(s)\cdots A_n(s)}{B_m(s)\cdots B_n(s)} \\ & \times\left[K_1 \cdots K_{m-1}\frac{A_1(s)\cdots A_{m-1}(s)}{B_1(s)\cdots B_{m-1}(s)}\right. \\ & \left.\times\left(\frac{e_{o_n}Z_a(s)}{Z_a(s) + Z_w(s)} - \frac{e_{o_n}Z_c(s)}{Z_c(s) + Z_b(s)}\right) + e_S\right]. \end{aligned} \tag{13}$$

Equation (13) implies that a minimum of two equivalent amplifier stages are needed to properly account for the introduction of offset voltage perturbations. The first of these two equivalent amplifiers, $a$, has a transfer function equal to the amplifier cascade up to (but not including) the $m$th amplifier where the offset voltage is injected, that is,

$$\frac{e_{o_a}}{e_{i_a}} = K_1 \cdots K_{m-1}\frac{A_1(s)\cdots A_{m-1}(s)}{B_1(s)\cdots B_{m-1}(s)} \tag{14}$$

or

$$\frac{e_{o_a}}{e_{i_a}} = K_a \frac{A_a(s)}{B_a(s)}. \tag{15}$$

The second equivalent amplifier, $b$, has a transfer function equivalent to the amplifier cascade from the $m$th to the $n$th amplifier, that is,

$$\frac{e_{o_b}}{e_{i_b}}(s) = K_m \cdots K_n \frac{A_m(s) \cdots A_n(s)}{B_m(s) \cdots B_n(s)} \tag{16}$$

or

$$\frac{e_{o_b}}{e_{i_b}} = K_b \frac{A_b(s)}{B_b(s)}. \tag{17}$$

The transfer function of the system response to offset voltage fluctuations using the equivalent amplifiers $a$ and $b$ is obtained from (13) as

$$\frac{e_{o_n}}{e_S}(s) = K_e \frac{Q_e(s)}{P(s)} \tag{18}$$

where $K_e = K_b$, the polnomial expression for the system zeros is given by

$$Q_e(s) = A_b(s)B_a(s)Z_1(s), \tag{19}$$

and the polynomial expression for the system poles is given by

$$P(s) = B_a(s)B_b(s)Z_1(s) + K_aK_bA_a(s)A_b(s)Z_2(s), \tag{20}$$

where

$$Z_1(s) = \left[Z_{a_N}(s)Z_{w_D}(s) + Z_{a_D}(s)Z_{w_N}(s)\right] \times \left[Z_{b_N}(s)Z_{c_D}(s) + Z_{b_D}(s)Z_{c_N}(s)\right] \tag{21}$$

and

$$Z_2(s) = Z_{a_D}(s)Z_{b_D}(s)Z_{c_N}(s)Z_{w_N}(s) - Z_{a_N}(s)Z_{b_N}(s)Z_{c_D}(s)Z_{w_D}(s). \tag{22}$$

Note that the poles of the amplifiers that precede the offset voltage injection stage appear as zeros in the overall system transfer for offset voltage fluctuations in Eq. (19). This is an important result, and the implications will be discussed later.

### System Transfer Function for Velocity Fluctuations

For the case of velocity fluctuations, the wire acts as the source of the voltage fluctuations and the total current perturbation $i_1$ depends on the nature of the impedances forming the wire arm of the bridge, $Z_w(s)$. The representation of $Z_w(s)$ required for the derivation of the transfer functions for velocity fluctuations is shown in Fig. 2. This representation does not restrict the generality implied by Eqs. (12), and an arbitrarily large number of elements can be used to form the impedances $Z_s(s)$, $Z_{wire}(s)$, and $Z_p(s)$.

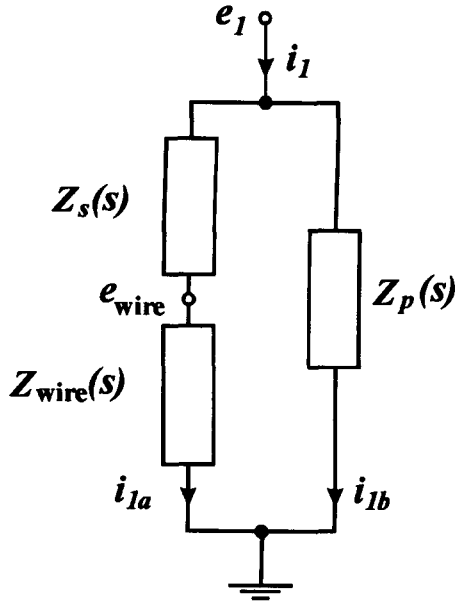


**Figure 2.** General representation of bridge impedance $Z_w$ required to derive the system transfer function for velocity fluctuations.

Let the transfer functions representing the impedance be given by

$$Z_{wire}(s) = \frac{Z_{wire_N}(s)}{Z_{wire_D}(s)}, \qquad Z_s(s) = \frac{Z_{s_N}(s)}{Z_{s_D}(s)}, \qquad Z_p(s) = \frac{Z_{pN}(s)}{Z_{pD}(s)}. \tag{23}$$

The voltage perturbation across the wire is given by

$$e_{wire} = Z_{wire}(s)i_{1a} + S_uF_u(s)u, \tag{24}$$

where $i_{1a}$ is the wire current, $S_u$ is the sensitivity to velocity perturbations (i.e., $\partial E_{wire}/\partial U$) at zero frequency, $u$ is the velocity perturbation, and $F_u(s)$ represents the normalized frequency response characteristics of the wire, that is, $F_u(0) = 1$. For a fixed mean velocity, $S_u$ is a constant. The voltage perturbation across the wire arm of the bridge is given by

$$e_1 = [Z_s(s) + Z_{wire}(s)]i_{1a} + S_uF_u(s)u, \tag{25}$$

which is also equal to the voltage perturbation across the parallel impedance,

$$e_1 = Z_p(s)i_{1b}. \tag{26}$$

The total perturbation current ($i_1 = i_{1a} + i_{ib}$) can be found from Eqs. (25) and (26), so the voltage perturbation at the top of the bridge can be determined:

$$e_{o_n} = [Z_a(s) + Z_w(s)]i_1 + S_uF_u(s)F_z(s)u, \tag{27}$$

where

$$F_z(s) = \frac{Z_p(s)}{Z_p(s) + Z_s(s) + Z_{wire}(s)} \tag{28}$$

and the impedance of the wire arm of the bridge is given by

$$Z_w(s) = \frac{Z_p(s)[Z_s(s) + Z_{wire}(s)]}{Z_p(s) + Z_s(s) + Z_{Wire}(s)}. \tag{29}$$

Substituting for $i_1$ from Eq. (27) and $i_2$ from Eq. (11) into Eq. (9) and using the two-amplifier model for the cascade, the system transfer function for velocity fluctuations is given by

$$\frac{e_{o_n}}{u}(s) = K_u \frac{Q_u(s)}{P(s)}, \tag{30}$$

where

$$K_u = S_u K_a K_b \tag{31}$$

and

$$Q_u(s) = A_a(s)A_b(s)Z_3(s)F_u(s)Z_{wire_D}(s), \tag{32}$$

where

$$Z_3(s) = Z_{a_N}(s)Z_{p_N}(s)Z_{s_D}(s) \times \left[Z_{b_N}(s)Z_{c_D}(s) + Z_{b_D}(s)Z_{c_N}(s)\right]. \tag{33}$$

The behavior of a hot-wire filament is very complex. For example, Perry [5] discusses aeroelastic effects and perturbations in the symmetry of the temperature distribution along the wire. Even relatively simple models that allow for a nonuniform temperature distribution along the wire must use a partial differential equation in space and time, which is beyond the scope of Laplace transform methods. In order to keep the analysis tractable a simple lumped model must be used for the hot-wire filament:

$$F_u(s) = \frac{1}{T_w s + 1} \tag{34}$$

and

$$\frac{Z_{wire_N}(s)}{Z_{wire_D}(s)} = \frac{R_w T_w S + R_w + \alpha}{T_w S + 1}, \tag{35}$$

where $T_w$ is the lumped time constant of the wire arising from its thermal inertia, $R_w$ is the dc wire resistance, and $\alpha = R_w(R_w - R_g)/R_g$, where $R_g$ is the wire resistance at gas temperature. The simple lumped model for the filament possesses the same time constant for the simple poles of the sensitivity to velocity and current fluctuations, and this leads to a simplified expression for the system zeros,

$$Q_u(s) = A_a(s)A_b(s)Z_3(s). \tag{36}$$

In the limit $Z_p(s) \to \infty$ (i.e., when there are no elements in parallel with the wire), the expression for $Z_3(s)$ given by Eq. (33) should not be used because it implies that $Q_u(s) \to \infty$. The expressions for $Z_1$(s) and $Z_2$(s) given by Eqs. (21) and (22) can be factored by $Z_{p_N}(s)$, and when $Z_p(s) = \infty$ the expression for $Z_3(s)$ is given by

$$Z_3(s) = Z_{a_N}(s)Z_{s_D}(s)\left[Z_{b_N}(s)Z_{c_D}(s) + Z_{b_D}(s)Z_{c_N}(s)\right]. \tag{37}$$

Equations (21) and (22) can still be used to evaluate $Z_1(s)$ and $Z_2(s)$ when $Z_p(s) = \infty$.

It is important to note that the poles of the transfer functions for both offset and velocity fluctuations are identical [provided that $F_u(s)Z_{wire_D}(s) = 1$]. This result is completely general in the sense that the system poles are identical independent of the number of amplifiers in the cascade, the complexity of the overall transfer function for the feedback amplifier, and the number of lumped components used to model the bridge impedances.

## SOME ILLUSTRATIVE EXPANSIONS OF TRANSFER FUNCTIONS

Unlike the poles, the zeros of the transfer function for offset and velocity fluctuations are quite different. It has already been proved that the poles of amplifiers preceding the offset voltage control stage appear as zeros in the transfer function for offset voltage perturbations but not for the velocity fluctuations. Other differences between the zeros of the two system transfer functions depend on the nature of the bridge impedances, and these will be considered in the examples below. It should be emphasized that the expansion of the polynomial expressions for the system poles from Eq. (20) and zeros from Eqs. (19) and (36) can be quite involved, even for relatively simple configurations. It is instructive to consider some particular cases.

### The Simplest Possible Configuration

For the simplest possible configuration, only resistive elements appear in the bridge, that is,

$$Z_{a_N}(s) = R_a, \qquad Z_{a_D}(s) = 1, \tag{38}$$

$$Z_{b_N}(s) = R_b, \qquad Z_{b_D}(s) = 1, \tag{39}$$

$$Z_{c_N}(s) = R_c, \qquad Z_{c_D}(s) = 1, \tag{40}$$

and from (35) and (12) the impedance of the wire arm of the bridge is given by

$$Z_{w_N}(s) = R_w T_w s + R_w + \alpha, \qquad Z_{w_D}(s) = T_w s + 1. \tag{41}$$

Substituting Eqs. (38)–(41) into (21), (22), and (37) leads to the expressions

$$Z_1(s) = (R_b + R_c)[(R_a + R_w)T_w s + (R_a + R_w + \alpha)], \tag{42}$$

$$Z_2(s) = \mathring{R}(T_w s + 1) + R_c \alpha, \tag{43}$$

$$Z_3(s) = R_a(R_b + R_c). \tag{44}$$

Assuming an ideal amplifier—one with infinite frequency response—then

$$A_a(s) = B_a(s) = A_b(s) = B_b(s) = 1. \tag{45}$$

Let the feedback amplifier consist of two stages such that $K_a = 1$ and $K_b = K$. Substitution of Eqs. (42)–(45) into (19), (20), and (36) leads to

$$Q_e(s) = (R_a + R_w)(R_b + R_c)T_w s + (R_a + R_w + \alpha)(R_b + R_c), \tag{46}$$

$$Q_u(s) = R_b + R_c, \tag{47}$$

$$P(s) = \left[(R_b + R_c)(R_a + R_w) + K\mathring{R}\right]T_w s + (R_b + R_c)(R_a + R_w + \alpha) + K\left(\mathring{R} + R_c + \alpha\right). \tag{48}$$

The time constant of the simple zero in (46) is approximately the same as the time constant $T_w$ of the wire filament. It is this zero that causes the system response to a step input of offset voltage to appear like the response expected from a delta function impulse of velocity. Note that this system possesses only one simple pole, so the step response can only exhibit an exponential decay, that is, the system response cannot exhibit ringing. The static response and the dynamic response are coupled through the quantity $\mathring{R}$, which is controlled by adjusting the offset voltage. Consideration of Eqs. (6) and (48) indicates that the time constant of the simple pole approaches zero (i.e., the frequency response of the system becomes infinite) as the offset voltage approaches zero. In practice, the frequency response is limited by other higher order effects as shown in the examples below.

The influence of the feedback amplifier was first considered by Ossowski [6], and for some time it was believed that the frequency response characteristics of the feedback amplifier were the dominant factor in the determination of overall system performance and stability. However, Davis and Davies [7] demonstrated that the inductance of the probe cable and the offset voltage of the feedback amplifier were the dominant parameters affecting stability and frequency response. Perry and Morrison [2] extended this work, and the results for a system with inductive bridge elements is expanded in the next section.

### Hot-Wire System with Inductance

Perry and Morrison [2] modeled the hot-wire cable as a simple lumped inductive element $L_w$ in series with the wire. Equations (35) and (12) give the components of impedance of the wire arm of the bridge as

$$\begin{aligned} Z_{w_N}(s) &= L_w T_w s^2 + (R_w T_w + L_w)s + (R_w + \alpha), \\ Z_{w_D}(s) &= T_w s + 1. \end{aligned} \tag{49}$$

Perry and Morrison demonstrated that the system stability and frequency response could be improved by incorporating a tunable balance inductor $L_b$ in series with the bridge resistor $R_b$. From (12), the components of the impedance of this arm of the bridge are

$$Z_{b_N}(s) = L_b s + R_b. \quad \text{and} \quad Z_{b_D}(s) = 1. \tag{50}$$

The upper bridge elements are purely resistive, and substitution of Eqs. (38), (40), (49), and (50) into Eqs. (21), (22), and (37) leads to the expressions

$$\begin{aligned} Z_1(s) = {} & L_b L_w T_w s^3 + \{[(R_b + R_c)L_w \\ & + (R_a + R_w)L_b]T_w + L_b L_w\}s^2 \\ & + \{(R_b + R_c)[(R_a + R_w)T_w + L_w] \\ & + (R_a + R_w + \alpha)L_b\}s \\ & + (R_b + R_c)(R_a + R_w + \alpha) \end{aligned} \tag{51}$$

$$\begin{aligned} Z_2(s) = {} & (R_c L_w - R_a L_b)T_w s^2 \\ & + \left(\mathring{R}T_w + R_c L_w - R_a L_b\right)s + \left(\mathring{R} + R_c\alpha\right), \end{aligned} \tag{52}$$

$$Z_3(s) = R_a[L_b s + (R_b + R_c)]. \tag{53}$$

Perry and Morrison [2] did not include the frequency response characteristics of the feedback amplifier so that the poles and zeros are given by (45). Substitution of these expressions into (20) for $P(s)$ leads to a third-order polynomial for the system poles,

$$P(s) = P_3 s^3 + P_2 s^2 + P_1 s + P_0, \tag{54}$$

where the constants $P_0, \ldots, P_3$ are given by

$$\begin{aligned} \begin{pmatrix} P_0 \\ P_1 \\ P_2 \\ P_3 \end{pmatrix} = {} & \begin{pmatrix} 1 & 0 & 0 & 0 \\ 0 & 1 & 0 & 0 \\ 0 & 0 & 1 & 0 \\ 0 & 0 & 0 & 1 \end{pmatrix} \begin{pmatrix} C_0 \\ C_1 \\ C_2 \\ C_3 \end{pmatrix} \\ & + K \begin{pmatrix} 1 & 0 & 0 \\ 0 & 1 & 0 \\ 0 & 0 & 1 \\ 0 & 0 & 0 \end{pmatrix} \begin{pmatrix} C_{K0} \\ C_{K1} \\ C_{K2} \end{pmatrix}, \end{aligned} \tag{55}$$

and $C_0, \ldots, C_3$ and $C_{K0}, \ldots, C_{K2}$ are constants that depend on the system parameters,

$$\begin{aligned} C_0 &= (R_b + R_c)(R_a + R_w + \alpha), \\ C_1 &= (R_b + R_c)[(R_a + R_w)T_w + L_w] \\ &\quad + (R_a + R_w + \alpha)L_b, \\ C_2 &= [(R_b + R_c)L_w + (R_a + R_w)L_b]T_w + L_b L_w, \\ C_3 &= L_b L_w T_w, \\ C_{K0} &= \mathring{R} + R_c\alpha, \\ C_{K1} &= \mathring{R}T_w + R_c L_w - R_a L_b, \\ C_{K2} &= (R_c L_w - R_a L_b)T_w. \end{aligned} \tag{56}$$

A single zero occurs in the transfer function for velocity fluctuations,

$$Q_u(s) = R_a(L_b s + R_b + R_c). \tag{57}$$

In most configurations this zero is located well beyond the frequency range of interest, so it is not of great significance. The expression for the zeros of the transfer function for offset voltage fluctuations is third-order

$$Q_e(s) = C_3 s^3 + C_2 s^2 + C_1 s + C_0. \tag{58}$$

The simple zero given by Eq. (46) for the simple system with only resistive bridge elements has a time constant that is approximately the same as that of the wire filament. It turns out that there is always a simple zero in Eq. (58) with a time constant of similar value. Therefore, the response to a step input will also appear like the response expected from a delta function impulse of velocity. However, the expression for the poles is now third-order, so a pair of complex conjugate poles are possible. In this case the step response may exhibit ringing, the decaying sinusoidal response that operators of hot-wire anemometers are familiar with.

Perry and Morrison proposed that the frequency response of the feedback amplifier can be omitted from a model of the system behavior because they found that it exerts only a small influence on the overall frequency response of the system. However, later, in the section on examples of fifth-order system behavior it shows that the frequency response of the feedback amplifier must be included to fully account for the behavior observed in real systems.

### Frequency Response Characteristics of the Feedback Amplifier

As mentioned previously, the influence of the frequency response characteristics of the feedback amplifier was first considered by Ossowski [6]. More recently, Freymuth [8] derived a model in which the frequency response of the feedback amplifier was controlled by adjusting the roll-off frequency of two simple poles. However, Freymuth did not account for the inductance of the probe cable, which has been shown to exert a dominant influence. Wood [9] derived a fifth-order model, including the amplifier characteristics in addition to the lumped inductance described in the previous subsection. The analysis of Wood will be discussed further later.

The positions of the system poles on the $s$ plane are independent of how the poles and zeros are distributed among the first and second equivalent amplifiers. However, extra zeros will appear in the transfer function for offset voltage fluctuations if the poles are located before the offset voltage control stage, $B_a(s)$; see Eq. (19). The number of zeros in the transfer function for velocity fluctuations remains unaltered in this situation; see Eq. (36). Further, any zeros that are incorporated into the feedback amplifier will appear in both system transfer functions only if they are added to the second equivalent amplifier. If any poles and/or zeros are deliberately added to the feedback amplifier for control purposes, then it is highly recommended that they be added only to the second equivalent amplifier, that is, after the offset voltage injection stage. This will avoid introducing any further differences between the system transfer functions for velocity and offset voltage fluctuations. The inherent differences between the transfer functions already make it difficult enough to correctly infer the system frequency response from square-wave tests.

$$\frac{e_{o_b}}{e_{i_b}}(s) = K_b \frac{M_1 s + 1}{(M_2 s + 1)(M_3 s + 1)}. \tag{59}$$

The first equivalent amplifier will be modeled using $A_a(s) = B_a(s) = 1$. This configuration could be used for examination of systems in which the gain of the feedback amplifier is frequency-dependent by putting $M_2 > M_1 > M_3$. The Bode diagram of a feedback amplifier with this particular frequency-dependent gain distribution is sketched in Fig. 3. Smits and Perry [10] considered the behavior of systems with a feedback amplifier with a frequency-dependent gain (except that they did not account for the high-frequency roll-off (i.e., $M_3$). The implications of using a feedback amplifier with a frequency-dependent gain will be discussed later.

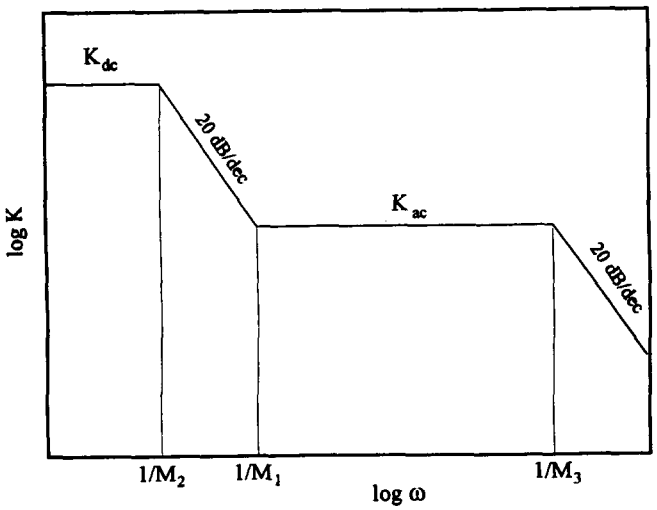


**Figure 3.** Sketch of Bode diagram for amplitude of a feedback amplifier with a simple zero with time constant $M_1$ and two simple poles with time constants $M_2$ and $M_3$.

This configuration of the feedback amplifier leads to a system in which the polynomial for the poles is fifth-order, that is,

$$P(s) = P_5 s^5 + P_4 s^4 + P_3 s^3 + P_2 s^2 + P_1 s + P_0, \tag{60}$$

where the constants $P_0, \ldots, P_t$ are given by

$$\begin{pmatrix} P_0 \\ P_1 \\ P_2 \\ P_3 \\ P_4 \\ P_5 \end{pmatrix} = \begin{pmatrix} 1 & 0 & 0 & 0 \\ M_2 + M_3 & 1 & 0 & 0 \\ M_2 M_3 & M_2 + M_3 & 1 & 0 \\ 0 & M_2 M_3 & M_2 + M_3 & 1 \\ 0 & 0 & M_2 M_3 & M_2 + M_3 \\ 0 & 0 & 0 & M_2 M_3 \end{pmatrix} \times \begin{pmatrix} C_0 \\ C_1 \\ C_2 \\ C_3 \end{pmatrix} + K \begin{pmatrix} 1 & 0 & 0 \\ M_1 & 1 & 0 \\ 0 & M_1 & 1 \\ 0 & 0 & M_1 \\ 0 & 0 & 0 \\ 0 & 0 & 0 \end{pmatrix} \begin{pmatrix} C_{K0} \\ C_{K1} \\ C_{K2} \end{pmatrix}. \tag{61}$$

The presentation of (61) using matrix notation has the advantage of being compact and demonstrates the coupling between the gain and the poles and zeros of the feedback amplifier. The expressions for the zeros can be obtained by multiplying the polynomials given by Eqs. (57) and (58) by $M_1 s + 1$. The extra zero given by $M_1 s + 1$ is cause for concern and will be discussed later.

### Additional Reactive Bridge Components

Including the frequency response characteristics of the feedback amplifier introduces a relatively small increase in the effort required to expand the transfer function polynomials. However, the addition of a small number of reactive bridge elements results in a much higher level of complexity. Using a single lumped inductor is a rather simplistic representation of a coaxial hot-wire cable with its distributed inductance, capacitance, resistance, and leakage conductance. A slightly more sophisticated model for the cable could include a lumped capacitor $C_w$ in parallel with lumped inductor $L_w$ and the wire. A balance capacitor $C_b$ could be introduced in parallel with the balance resistor and balance inductor. This configuration was originally derived by Watmuff [3] and leads to a system in which the polynomial for the poles is seventh-order, that is,

$$P(s) = P_7 s^7 + P_6 s^6 + P_5 s^5 + P_4 s^4 + P_3 s^3 + P_2 s^2 + P_1 s + P_0, \tag{62}$$

where the constants $P_0, \ldots, P_7$ are given by

$$\begin{pmatrix} P_0 \\ P_1 \\ P_2 \\ P_3 \\ P_4 \\ P_5 \\ P_6 \\ P_7 \end{pmatrix} = \begin{pmatrix} 1 & 0 & 0 & 0 & 0 & 0 \\ M_2+M_3 & 1 & 0 & 0 & 0 & 0 \\ M_2M_3 & M_2+M_3 & 1 & 0 & 0 & 0 \\ 0 & M_2M_3 & M_2+M_3 & 1 & 0 & 0 \\ 0 & 0 & M_2M_3 & M_2+M_3 & 1 & 0 \\ 0 & 0 & 0 & M_2M_3 & M_2+M_3 & 1 \\ 0 & 0 & 0 & 0 & M_2M_3 & M_2+M_3 \\ 0 & 0 & 0 & 0 & 0 & M_2M_3 \end{pmatrix} \begin{pmatrix} C_0 \\ C_1+C_1' \\ C_2+C_2' \\ C_3+C_3' \\ C_4' \\ C_5' \end{pmatrix} \tag{63}$$

$$+K \begin{pmatrix} 1 & 0 & 0 & 0 & 0 \\ M_1 & 1 & 0 & 0 & 0 \\ 0 & M_1 & 1 & 0 & 0 \\ 0 & 0 & M_1 & 0 & 0 \\ 0 & 0 & 0 & M_1 & 0 \\ 0 & 0 & 0 & 0 & M_1 \\ 0 & 0 & 0 & 0 & 0 \\ 0 & 0 & 0 & 0 & 0 \end{pmatrix} \begin{pmatrix} C_{K0} \\ C_{K1}+C_{K1}' \\ C_{K2}+C_{K2}' \\ C_{K3}' \\ C_{K4}' \end{pmatrix}.$$

The constants $C_0$, $C_1$, $C_2$, $C_3$, $C_{K0}$, $C_{K1}$, and $C_{K2}$ are given in (56), and

$$\begin{aligned}
C_1' &= R_bR_c(R_a+R_w+\alpha)C_b \\
&\quad + R_a(R_b+R_c)(R_w+\alpha)C_w, \\
C_2' &= R_a(R_b+R_c)(R_wT_w+L_w)C_w+R_a(R_w+\alpha)L_bC_w \\
&\quad + R_bR_c[(R_a+R_w)T_w+L_w]C_b \\
&\quad + R_c(R_a+R_w+\alpha)L_bC_b \\
&\quad + R_aR_bR_c(R_w+\alpha)C_bC_w, \\
C_3' &= R_a(R_b+R_c)L_wT_wC_w \\
&\quad + R_a(R_wT_w+L_w)L_bC_w \\
&\quad + R_c[(R_a+R_w)T_w+L_w]L_bC_b + R_bR_cL_wT_wC_b \\
&\quad + R_aR_bR_c(R_wT_w+L_w)C_bC_w \\
&\quad + R_aR_c(R_w+\alpha)L_bC_bC_w, \\
C_4' &= R_aR_c[(R_wL_b+R_bL_w)T_w+L_bL_w]C_bC_w \\
&\quad + (R_cC_b+R_aC_w)L_bL_wT_w, \\
C_5' &= R_aR_cL_bL_wT_wC_bC_w, \\
C_{K1}' &= R_b(R_w+\alpha)(R_cC_b-R_aC_w), \\
C_{K2}' &= [L_b(R_w+\alpha)+R_b(R_wT_w+L_w)](R_cC_b-R_aC_w), \\
C_{K3}' &= [(R_wL_b+R_bL_w)T_w+L_bL_w](R_cC_b-R_aC_w), \\
C_{K4}' &= L_bL_wT_w(R_cC_b-R_aC_w).
\end{aligned} \tag{64}$$

The zeros for offset voltage perturbations are given by

$$\begin{aligned}
Q_e(s) &= (M_1s+1)[C_5's^5+C_4's^4+(C_3+C_3')s^3 \\
&\quad +(C_2+C_2')s^2+(C_1+C_1')s+C_0],
\end{aligned} \tag{65}$$

and the zeros for velocity fluctuations are given by

$$\begin{aligned}
Q_u(s) &= R_a(M_1s+1)[L_bC_bs^2+(R_bR_cC_b+L_b)s \\
&\quad +R_b+R_c].
\end{aligned} \tag{66}$$

It is significant that the terms $(R_cL_w - R_aL_b)$ and $(R_cC_b - R_aC_w)$ appear in the expressions for the transfer function coefficients given by Eqs. (56) and (64) because the influence of the reactive bridge elements can be minimized if these terms approach zero. For both of these terms to be zero requires that $L_b/L_w = R_c/R_a =$ (cross-bridge ratio) and that $C_b/C_w = R_a/R_c = 1/$(cross-bridge ratio). This means that the only way to nullify both of these terms is to make the cross-bridge ratio unity. This may be the reason a symmetrical bridge is offered as an option for high-frequency operation with one commercially available system.

## Discussion

Wood [9] performed an analysis of the type of system in which the gain of the feedback amplifier is frequency-dependent. For systems with a frequency-dependent gain, the term $K\mathring{R}$ is multiplied by the ratio of the ac gain to the dc gain, which can be as small as 0.003. This minimizes the effect of offset voltage, and the system stability and frequency response are adjusted by varying the ac gain in conjunction with the balance inductance and roll-off frequency of the amplifier. This is typical of some commercially available systems and is thought to offer several advantages over systems using a feedback amplifier with a flat frequency response. First, tuning the system frequency response by adjusting the ac gain does not alter the hot-wire calibration like offset voltage adjustment does. However, if the frequency response and stability of the system are properly tuned, then there should be no need for further adjustments after calibration. Second, as mentioned above, a constant-temperature hot-wire anemometer cannot maintain the bridge in perfect balance. The

wire resistance varies slightly with mean velocity, so the calibration curve deviates from the ideal constant-temperature behavior. Systems with high dc gain amplifiers are designed to minimize the bridge imbalance, so the hot-wire system can be thought to more closely follow some idealized heat transfer law, such as King's law.

Smits and Perry [10] studied the influence of the overall gain by assuming King's law and solving (4) and (5) for the operating point as the velocity is varied. They found that the deviations from ideal behavior were of the order of 1% for a gain of 500 and that increasing the gain beyond 1000 brings only a diminishing return. These small deviations from ideal behavior would be accounted for in practice by the curve fit used for the calibration. In any case, a hot-wire filament cannot be regarded as a straight infinitely long cylinder of uniform circumferential and spanwise temperature (see Perry [5]), so it seems unlikely that there exists a single universal heat transfer law for hot-wire calibrations. When these practical considerations are taken into account, the advantage of frequency-dependent gain systems should be considered idealistic and of minor significance.

Of more concern is that a negative step in the Bode diagram occurs when the feedback amplifier has a frequency-dependent gain. In his paper, Wood [9] states, "the theory presented here for the a.c. response holds only for frequencies above that at which the a.c. gain becomes flat." Although he could not calculate the response from his analysis in the frequency range where the amplifier gain is falling from its dc level to its ac plateau, Wood realized that a significant step in the frequency response could occur. He argued, by worst case example, that the effect is important (7%) only at low resistance ratios and for low ac gains. However, Smits and Perry [10] found that the step size can be significant for resistance ratios greater than 1.1. Even for resistance ratios on the order of 1.5 they showed that the size of the step can be as large as 3% of the static response. For these reasons, the feedback amplifier of the anemometer considered in the examples below will have a flat frequency response, $M_1 = 0$. The time constants $M_2$ and $M_3$ will be treated as variables for adjusting the roll-off frequency of the feedback amplifier.

## COMPUTER SIMULATIONS

The expansions given above illustrate that the derivation of transfer functions for even high-order systems would be extremely tedious, particularly for systems with large numbers of reactive bridge elements. One way to avoid the tedious algebra would be to derive the transfer functions using a symbolic manipulation software package. However, this would require a commitment to the highest level of complexity to be studied before invoking the derivation. An alternative method that avoids this restriction consists of deriving the transfer functions numerically. One disadvantage of the numerical method compared to the symbolic manipulation software approach is that the relationships between the parameters forming the coefficients of the transfer function polynomials are hidden. However, the analytical expressions for the polynomial coefficients for higher order systems approach such complexity that little can be inferred by direct examination anyway.

Computer simulations are a convenient tool for exploring the behavior of hot-wire systems because the trajectories of the poles and zeros on the $s$ plane, the Bode diagrams, and the square-wave response can all be calculated for each operating point as the anemometer controls are adjusted. In a real system the operator can view only the square-wave response. A computer simulation allows operating conditions to be examined that are beyond current technology, and extreme operating conditions can be explored without the penalty of wire breakage.

An interactive program has been written for examining the stability and frequency response of constant-temperature hot-wire systems. All the parameters can be specified via menus, including the number and type of components forming the impedance of each arm of the bridge and the fluid and wire properties. The poles and zeros of the two equivalent amplifiers for the feedback can be specified, and the amplifier transfer function polynomials are calculated using Eqs. (14) and (16). For a given set of parameters, the static operating point is obtained by iteration using Eqs. (4) and (5). The Nusselt number is evaluated using Kramer's relationship. For the results presented here, the convergence tolerance for $I_1$ is one part in $10^{-4}$. The lumped time constant $T_w$ and the operating resistance of the wire are evaluated using expressions given in Perry [5]. The impedance of each arm of the bridge is then calculated as the ratio of two polynomials as expressed in Eqs. (12). The coefficients of $Z_1(s)$, $Z_2(s)$, and $Z_3(s)$ given by Eqs. (21), (22), and (37) [or Eq. (33) if there are elements in parallel with the wire] are calculated using general-purpose routines for multiplying and adding polynomials. These routines are then used to calculate the coefficients of the polynomial expressions for the transfer function zeros $Q_e(s)$ and $Q_u(s)$ using Eqs. (19) and (36) and for the poles $P(s)$ using Eq. (20). The roots of the transfer function polynomials (i.e., the poles and zeros) are found numerically using the Lin–Bairstow method of successive quadratic factorization. The calculations were performed using Fortran Real*16 and Complex*16 variables, and the accuracy of the pole and zero estimation was typically one part in $10^{15}$.

If the system input (i.e., $u$ or $e_s$) is sinusoidal, then the output will also be sinusoidal after a sufficient time has elapsed for the transients to have decayed. This corresponds to putting $s = j\omega$ in the transfer function, which gives a complex number for $e_o/e_s$ and $e_o/u$. The absolute values $|e_o/e_s|$ and $|e_o/u|$ give the Bode diagrams for amplitude. The response to a more general class of inputs is given by Perry [5], and this has been used to calculate the square-wave response.

## INTERPRETATION OF ELECTRONIC SQUARE-WAVE TESTS

It is again emphasized here that one of the additional zeros in the system transfer function for offset voltage perturbations is always a simple zero with a time constant close to that of the wire filament. The time constants of the system poles are usually at least an order of magnitude smaller than this zero. Consequently, the dc component of the system response to a step input of offset voltage is greatly diminished with respect to the higher frequency components. Therefore, this simple zero is responsible for causing the electronic square-wave response

to have an appearance resembling that expected from a delta function impulse of velocity.

The characteristic frequency of a pole is equal to the scalar distance of the pole from the origin of the $s$ plane. When there is more than one pole in the system, the frequency response or "roll-off" frequency of the system will be defined to be equal to the lowest characteristic frequency of all the system poles. The pole(s) possessing this characteristic frequency will be referred to here as the dominant pole(s). Although the system will respond to higher frequency inputs it is strictly unusable beyond this point because the system sensitivity varies with frequency.

The most common method for tuning anemometers is to first adjust the square-wave response such that it exhibits optimally damped second-order behavior and then estimate the frequency response from the ringing frequency. Although the square-wave test is an invaluable aid for tuning anemometers, it is easy to misinterpret the actual frequency response. Of particular concern is any simple pole that possesses a characteristic frequency that is lower than that of the complex conjugate poles. In this situation the square-wave response may still exhibit high-frequency oscillations, but these will be at a higher frequency than the system response, which is dominated by the simple pole. Examples are given in the next section that demonstrate the danger of blindly following a simplistic recipe for adjusting the frequency response.

## EXAMPLES OF FIFTH-ORDER SYSTEM BEVAVIOR

It has been my experience that the bare minimum configuration capable of reproducing the behavior observed in real systems is that defined in the section on frequency response characteristics of the feedback amplifier, which includes the frequency response characteristics of the feedback amplifier and the lumped inductor representing the probe cable and the balance inductor. Examples of undesirable modes of operation are demonstrated below, and instructions are given on how to avoid them by appropriate adjustment of the anemometer controls.

### Offset Voltage of the Feedback Amplifier

The results of a systematic parametric study suggest that only two types of dominant pole $s$-plane trajectories are observed as the amplifier offset voltage $E_{qi}$ is varied. The type of dominant pole trajectory depends on the nature of these poles as frequency response of the feedback amplifier $f_A \to \infty$. The effect of varying $E_{qi}$ on the higher order poles is usually very small.

Two examples that are representative of each type of behavior have been calculated. The frequency response of the feedback amplifier is assumed to be flat through to a simple second-order roll-off, that is, $M_1 = 0$ and $M_2 = M_3 = M$ in Eq. (59). In each example the gain $K$ and frequency response $f_A$ of the feedback amplifier are fixed at $K = 1000$ and $f_A \approx 79.6$ kHz (i.e., $M = 2 \times 10^{-6}$ s), and the trajectories of the system poles on the $s$ plane are traced out as the offset voltage $E_{qi}$ is varied. Only quadrant 2 of the $s$ plane is shown because quandrant 3 is the mirror image of 2 reflected about the real axis.

Initially, in the first example, at the point labeled 1 in Fig. 4, the system is dominated by a pair of complex

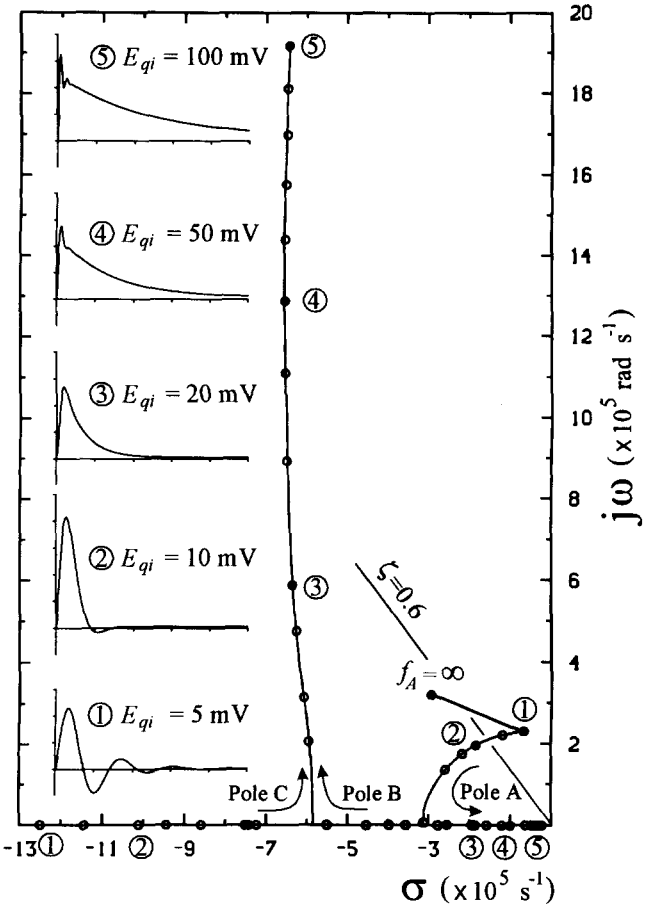


**Figure 4.** Calculated $s$-plane trajectories (second quadrant only) of dominant poles for fifth-order system with increasing offset voltage $E_{qi}$. Inductor values $L_b = 8$ $\mu$H, $L_w = 1$ $\mu$H, amplifier frequency response $f_A \approx 79.6$ kHz, and gain $K = 1000$ are constant. Flow velocity $U = 20$ m/s. Point $f_A = \infty$ corresponds to model to Perry and Morrison [2] (i.e., $M = 0$) for conditions at point 1. Square-wave response for operating points 1–5 also shown. Line $\zeta = 0.6$ shows optimum damping for complex poles.

conjugate poles labeled A (with image B). There is also a simple pole labeled C and another two higher order simple poles D and E; D and E remain well behaved and beyond the frequency range of interest, and their trajectories are not shown. Note that if the frequency response of the feedback amplifier were increased to infinity while the other parameters were held fixed, the system would still be dominated by a pair of complex conjugate poles, but they would be more damped as illustrated by the point labeled $f_A = \infty$ in Fig. 4. Increased damping of the dominant poles with increased $F_A$ appears to be a general property of constant-temperature hot-wire systems. This rather surprising property will be discussed in more detail later. Returning to conditions at point 1, as $E_{qi}$ is increased, the complex conjugate poles A and B move toward the real axis, where they eventually meet and split to form two simple poles. These points are known as breakaway points in the system theory literature. As $E_{qi}$ is further increased, the simple pole C, which has been moving toward the origin, now merges with the simple

pole B to form a new complex conjugate pair. However, pole A has continued to move closer to the origin, and therefore it dominates the system frequency response. This behavior is typical of systems in which the dominant poles remain complex as $f_A \to \infty$.

The square-wave response corresponding to the points labeled 1–5 are also shown in the figure. The square-wave response can be very misleading under these conditions. For example, for conditions corresponding to point 5 in Fig. 4, where $E_{qi} = 100$ mV, the ringing frequency is around 320 kHz, but the simple pole A limits the system frequency response to about 3.6 kHz. The Bode diagrams and the step response for both offset voltage perturbations and velocity fluctuations corresponding to this situation are shown in Fig. 5, and they clearly demonstrate why this type of system behavior is undesirable.

An example of the second type of trajectory is shown in Fig. 6. For conditions corresponding to point 1, the dominant poles are also complex conjugates. However, in the limit $f_A \to \infty$ this system possesses *all* simple poles, and different $s$-plane trajectories are observed as the offset voltage $E_{qi}$ is varied. With increasing $E_{qi}$, poles A and B remain complex conjugate while simple pole C moves toward to the origin and eventually dominates the system. This behavior is typical of systems that possess only simple poles when $f_A \to \infty$. Despite the different trajectories of the dominant poles, the end result is much the same as in the first example, and the system possesses similar undesirable Bode diagrams and step-response characteristics.

It turns out that for the third-order system considered by Perry and Morrison [2] (i.e., $f_A = \infty$, see the earlier section entitled "Hot-Wire System with Inductance"), the type of behavior observed in the above examples can only be produced when the balance inductor $L_b$ is set to be very close to the value required for ac bridge balance, $L_{b0} = (R_c/R_a)L_w$. For values of $L_b$ slightly less than this, the system is dominated by the usual complex conjugate pole pair. For values of $L_b$ slightly greater than $L_{b0}$, the poles rapidly cross over to the right half-plane and the system becomes unstable. However, in a real system the phenomena described above can be produced over a wide range of balance inductor settings by increasing the offset voltage $E_{qi}$. The only way to simulate these observations is to include the frequency response characteristics of the feedback amplifier.

## Balance Inductor

As mentioned above, the analysis of Perry and Morrison [2] predicts instability when the balance inductor $L_b$ is in excess of the value required for ac bridge balance $L_{b0}$. However, systems with finite frequency response amplifiers are capable of maintaining system stability when the balance inductor exceeds the ac balance value $L_{b0}$. For a fixed amplifier frequency response $f_A$ it is possible to obtain significant improvements in the system frequency response $f_0$ by suitably adjusting the offset voltage as $L_b$ is increased to values in excess of $L_{b0}$. In fact, having

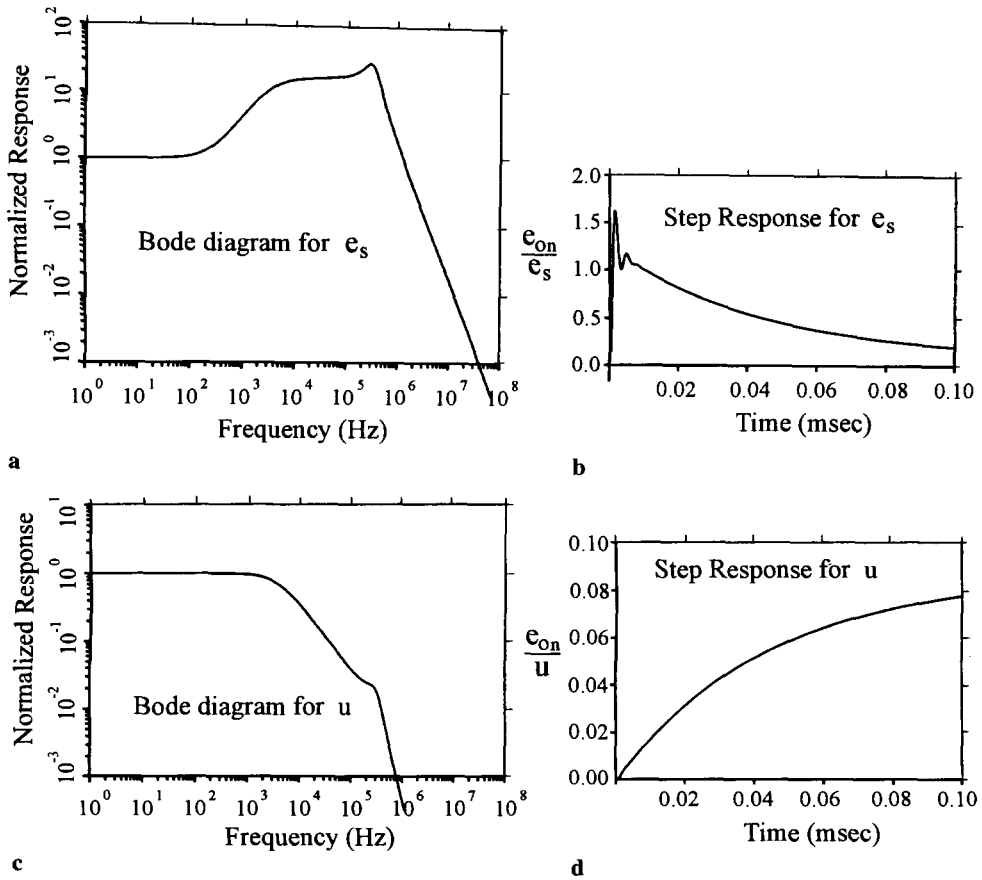


**Figure 5.** Bode diagrams and step-response for point 5 in Fig. 4 where $E_{qi} = 100$ mV. (*a*) and (*b*) offset voltage perturbations $e_S$, (*c*) and (*d*) for velocity fluctuations $u$.

control of only $E_{qi}$ and $L_b$ requires that $L_b > L_{b0}$ to obtain the optimum system response. However, if $L_b$ is too large it may be impossible to obtain a satisfactory response by adjusting the offset voltage.

$L_b/L_{b0} = 0.5$ in the example shown in Fig. 6, and this configuration will serve as a baseline from which to illustrate these effects. The $s$-plane trajectories for this configuration are reproduced in Fig. 7 along with those of five other configurations in which the values of $L_b/L_{b0}$ are held fixed at 1, 2, 3, 4, and 5, respectively. For small values of the offset voltage (e.g., $E_{qi} < 2$ mV), nearly all the configurations are unstable because the poles A (and B) are located on the right half-plane. As $E_{qi}$ is increased, these poles cross to the left half-plane and the simple pole C of each system moves along the real axis toward the origin. For a given offset voltage, the initial position of pole C is further from the origin for smaller values of $L_b$. However, this effect is pronounced only when $E_{qi}$ is small. As $E_{qi}$ is increased, the location of the simple poles C become more and more independent of $L_b$. For each $L_b$, the best response will be defined to be when the characteristic frequency (i.e., $|\sigma + j\omega|/2\pi$) of poles A and B and simple pole C are equal. For $L_b \leq L_{b0}$, the best response occurs when poles A (and B) are overdamped. When $L_b > L_{b0}$, poles A (and B) never reach the optimum damping condition, so the best response occurs when they are underdamped. The locus of the operating point with the best response that can be obtained by adjusting both the offset voltage $E_{qi}$ and the balance inductor $L_b$ is shown as a dashed curve. Optimum damping ($\zeta = 0.6$) occurs when $L_b \approx 1.5L_{b0}$. The square-wave response corresponding to various operating points is shown in Fig. 8,

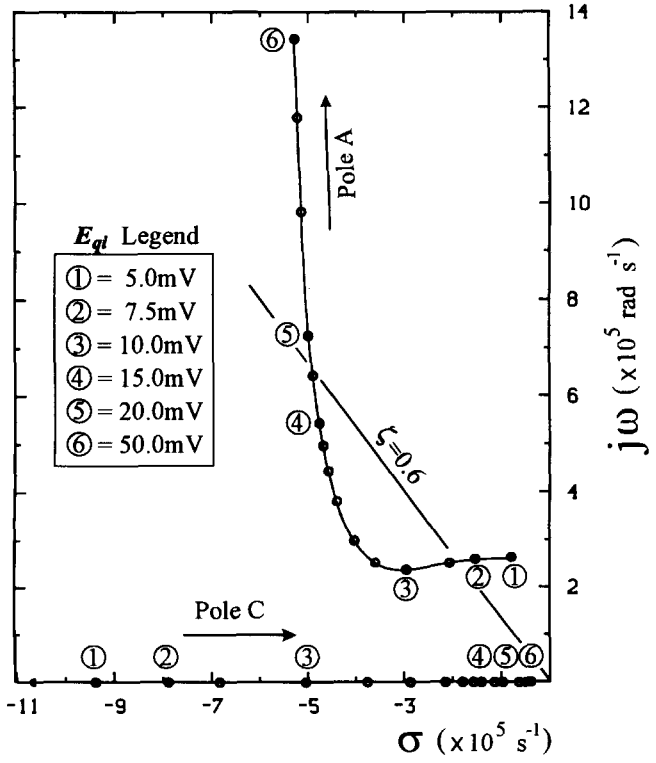


**Figure 6.** Same as Fig. 4 but with $L_b = 0.5$ $\mu$H and $L_w = 0.1$ $\mu$H. Despite the different $s$-plane trajectories, the end result is much the same as in Fig. 4 for large $E_{qi}$.

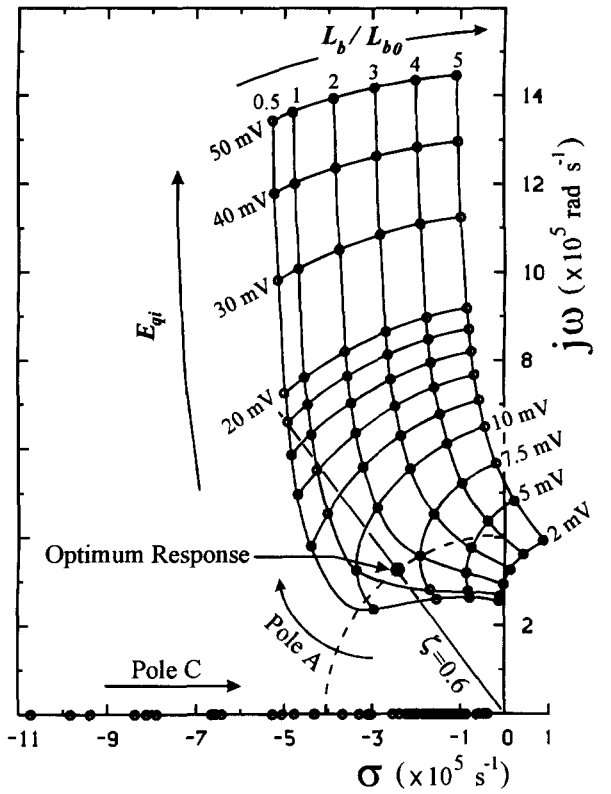


**Figure 7.** Same as Fig. 6 where $L_w = 0.1$ $\mu$H and $L_{b0} = (R_c/R_a)L_w = 1$ $\mu$H. Trajectories for $L_b/L_{b0} = 0.5$, 1, 2, 3, 4, and 5 also shown. Dashed line shows locus of points where poles A, (B), and C have equal characteristic frequencies. Having $E_{qi}$ and $L_b$ as the only tunable parameters leads to an optimum response when $L_b \approx 1.5$ $L_{b0}$.

and these may help operators interpret anemometer behavior. In particular, note how there is no adjustment of $E_{qi}$ that will increase the damping of system to a satisfactory level when $L_b$ is very large. An operator observing this type of square-wave response is advised to reduce the size of the balance inductor.

## Frequency Response and Gain of the Feedback Amplifier

Intuitively it might be expected that the roll-off frequency of the feedback amplifier would play a dominant role in determining the overall system frequency response. Analysis predicts that the frequency response of hot-wire systems $f_o \to \infty$ in the limits of $f_A \to \infty$, $K \to \infty$, $E_{qi} \to 0$, and $L_b \to L_{b0}$. However, attempts to approach these limits in practice are invariably frustrated by the appearance of instabilities. For example, Smits and Perry [10] observed that hot-wire systems are prone to instabilities as $L_b \to L_{b0}$ because there is an extreme sensitivity to very small variations in $L_b$. However, this observation was made for a third-order model where $f_A = \infty$. Systems with finite frequency response amplifiers have an optimum frequency response when $L_b > L_{b0}$, and stability can be maintained even when $L_b$ is excessively large. Nevertheless, one might suspect that the form of dominant pole instability described by Smits and Perry will eventually occur as $f_A$ is increased. However, the results of a system-

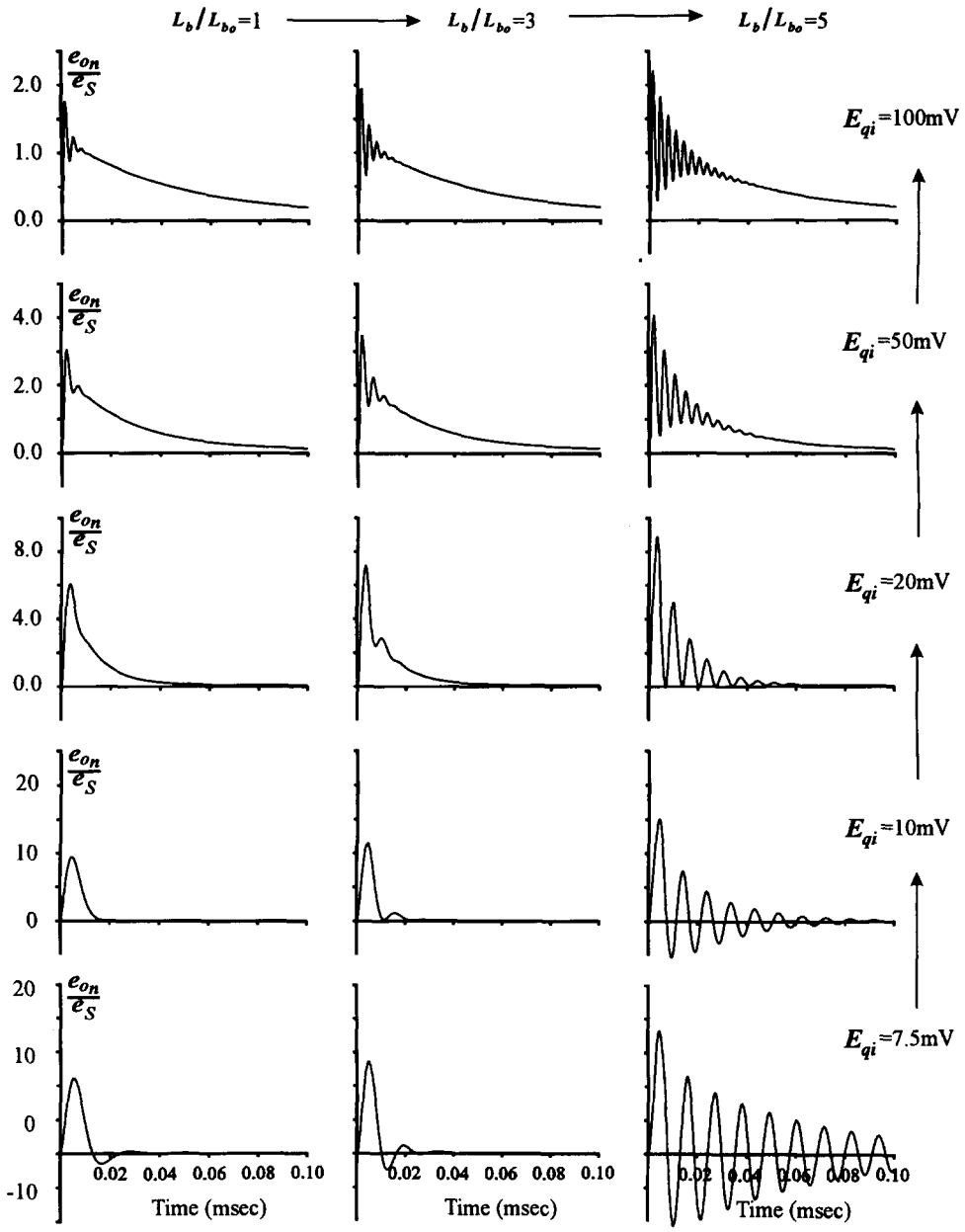


**Figure 8.** Square-wave response corresponding to a spread of points in Fig. 7. It is impossible to obtain a satisfactory response by adjusting $E_{qi}$ when $L_b/L_{b0}$ is excessive.

atic parametric study suggests that other higher order instabilities are more likely to arise beforehand. Although there are still significant improvements to be found by increasing the frequency response and gain of the amplifier, its role is often more critical in determining the system stability by influencing the higher order poles. Two examples are given in Figs. 9 and 10.

Calculated $s$-plane trajectories of a typical fifth-order system are shown in Fig. 9. Two cases are considered: increasing amplifier frequency response and increasing gain. The behavior of the dominant poles labeled A and B and the higher order poles labeled C, D, and E are shown separately in Figs 9*a* and 9*b* because of the wide range of values observed. In the first case, the amplifier gain $K$ = 1000, the offset voltage $E_{qi}$ = 12.5 mV, and the inductances $L_b$ = 40 $\mu$H and $L_w$ = 5 $\mu$H are held constant. Note that the damping of the dominant poles A and B increases with increasing amplifier frequency response. As a matter of interest, the system frequency response ($f_o \approx$ 17.8 kHz) is higher than the amplifier frequency response ($f_A \approx$ 15.9 kHz; i.e., $M = 1.0 \times 10^{-5}$s) for conditions corresponding to points labeled 1A in Fig. 9*a*. The system response increases rapidly with increasing amplifier frequency response but only to $f_o \approx$ 27 kHz for $f_A \approx$ 106 kHz (i.e., $M = 1.58 \times 10^{-6}$ s). Further increases in the amplifier frequency response have only a small effect on the dominant poles; for example, $f_o \rightarrow$ 31 kHz for $f_A \rightarrow \infty$ (i.e., $M \rightarrow 0$). As the amplifier frequency response is increased, two of the higher-order simple poles, C and D, move toward each other and merge to become complex

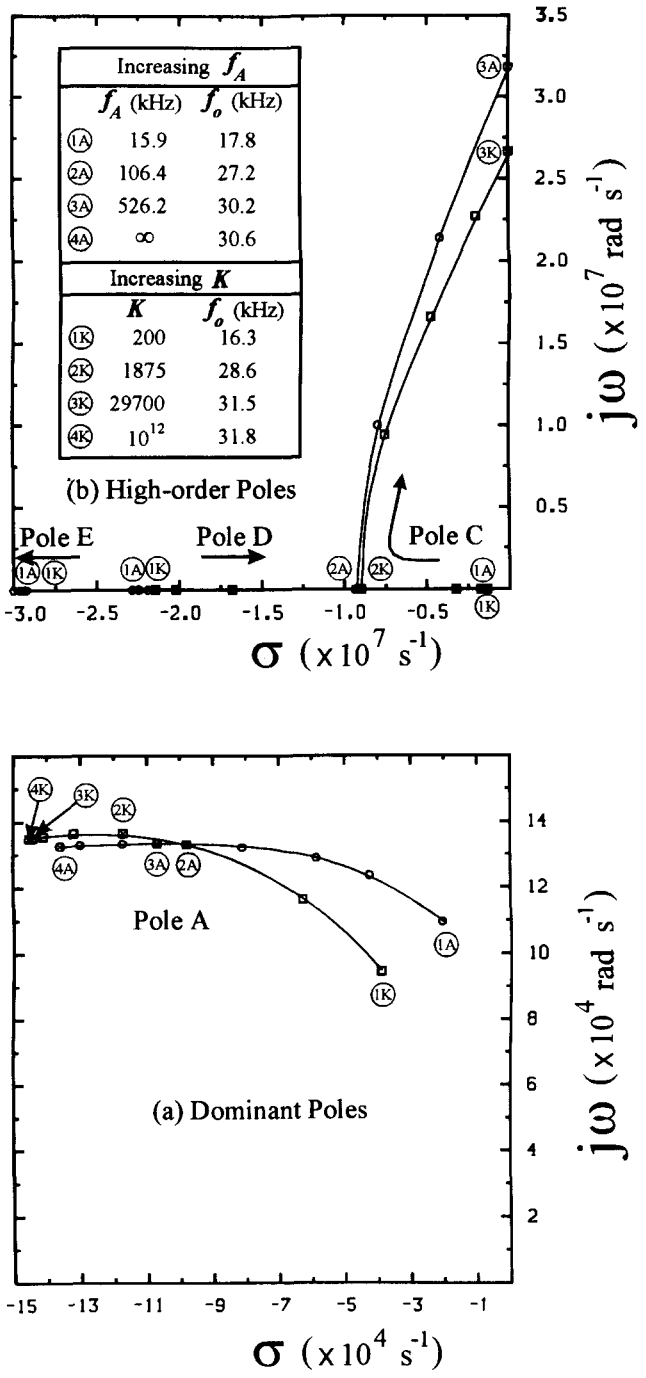


**Figure 9.** Calculated $s$-plane trajectories of system poles for increasing $f_A$ (with constant $K = 1000$) and for increasing $K$ (with constant $f_A \approx 79.6$ kHz). $E_{qi} = 12.5$ mV, $L_w = 5$ $\mu$H, and $L_b = 40$ $\mu$H. (*a*) Dominant poles; (*b*) higher order poles.

conjugates for $f_A \approx 106$ kHz. This breakaway point is labeled 2A in Fig. 9*b*. The third simple pole, E, moves further away from the origin and exerts negligible influence on the system. With further increases in the amplifier frequency response, the two higher order conjugate poles C and D move toward the imaginary axis and ultimately cross over to the right half-plane, resulting in instability.

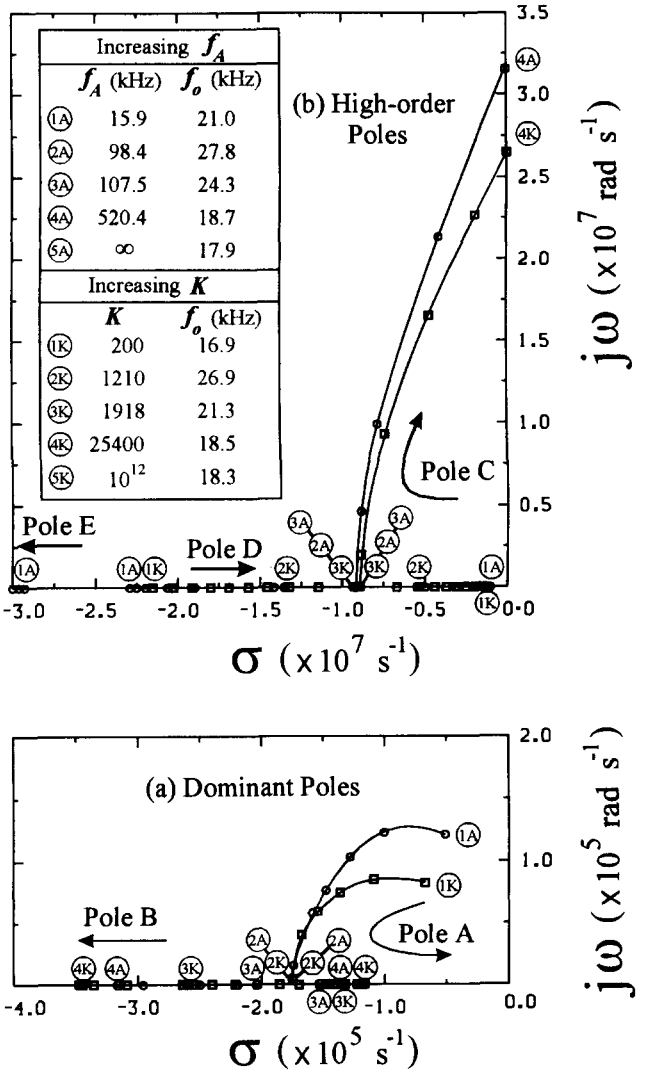


**Figure 10.** Same system as Fig. 8 but with $E_{qi}$ increased to 20 mV. Calculated $s$-plane trajectories of system poles for increasing $f_A$ (with constant $K = 1000$) and for increasing $K$ (with constant $f_A \approx 79.6$ kHz). (*a*) Dominant poles; (*b*) higher order poles.

Similar behavior is observed if the amplifier gain $K$ is increased while the other parameters ar held constant as shown in Fig. 9*b*. Although the dominant poles move along slightly different trajectories, the endpoints $K = \infty$ and $f_A = \infty$ are very closely the same. The $s$-plane trajectories of the higher order system poles C and D are very similar as $K \to \infty$ and $f_A \to \infty$.

In the previous example the dominant poles approach the complex conjugate third-order system values asymptotically as $K \to \infty$ and as $f_A \to \infty$. In the second example, shown in Fig. 10*a*, a different type of trajectory is observed. The dominant poles A and B move toward the real axis, where they meet and split to form two simple poles. These poles also approach the third-order system values asymptotically as $K \to \infty$ and as $f_A \to \infty$. This type of behavior is also consistent with the observation mentioned previously that relates the increased damping of the domi-

nant poles to increased frequency response and gain of the feedback amplifier. Note that increasing $f_A$ or $K$ beyond the point where the dominant complex poles are transformed into two simple poles actually reduces the overall system frequency response because pole A moves closer to the origin. The effects of increasing $K$ and $f_A$ on the higher order poles are very similar to those in the previous example, despite the different trajectories for the dominant poles; that is, the poles C and D merge to become complex conjugate and move toward the imaginary axis. The higher order poles ultimately cross over to the right half-plane, resulting in system instability as shown in Fig. 10*b*).

These examples demonstrate several important properties of constant-temperature hot-wire systems. The effects of increasing $K$ and $f_A$ are quite similar and have the unexpected effect of increasing the stability of the dominant poles. This appears to be true for all systems; not one contrary example has been found to this observation out of a large number of cases studied. It is the higher order poles that are responsible for the system instability under these conditions. It is often difficult to determine the damping of the higher order poles during a square-wave test even when they are grossly underdamped, because the oscillations can still decay rapidly compared to the response of the dominant poles. However, a small change in either $K$ or $f_A$ from this point could result in instability. This type of higher order instability can occur suddenly and without warning to the anemometer operator, who can only observe the square-wave response.

### Instabilities with Subminiature Wires

Some workers (e.g., Miller et al. [11]) have reported frustration with instabilities when using subminiature hot wires. One way of comparing system behavior with different diameter wires is to nondimensionalize the poles and zeros with the lumped time contant of the wire, $T_w$. Alternatively, the coefficients of $s^n$ in the system transfer functions can be made nondimensional by division by $R_w^2 T_w^n$. The relative positions of the nondimensional poles and zeros will be the same for systems in which $R_a/R_w$, $R_b/R_w$, $R_c/R_w$, $R/R_w^2$, $L_b/R_wT_w$, $L_w/R_wT_w$, and $M/T_w$ are equivalent.

For a given $l/d$ ratio, $R_g \propto d^{-1}$, so that $R_g$ for a typical subminiature wire (e.g., $d = 0.5$ $\mu$m) is about an order of magnitude greater than for a more conventional wire (e.g., $d = 5$ $\mu$m). $T_w$ is reduced for smaller diameter wires but by a smaller factor than the length-scale ratio because the Reynolds number is also reduced. Consequently, the product $R_wT_w$ becomes larger as the wire is made smaller. This leads to a beneficial reduction in the size of the nondimensional bridge inductance $L_b/R_wT_w$ and $L_w/R_wT_w$. Values of $R_a/R_w$, $R_b/R_w$, $R_c/R_w$, and

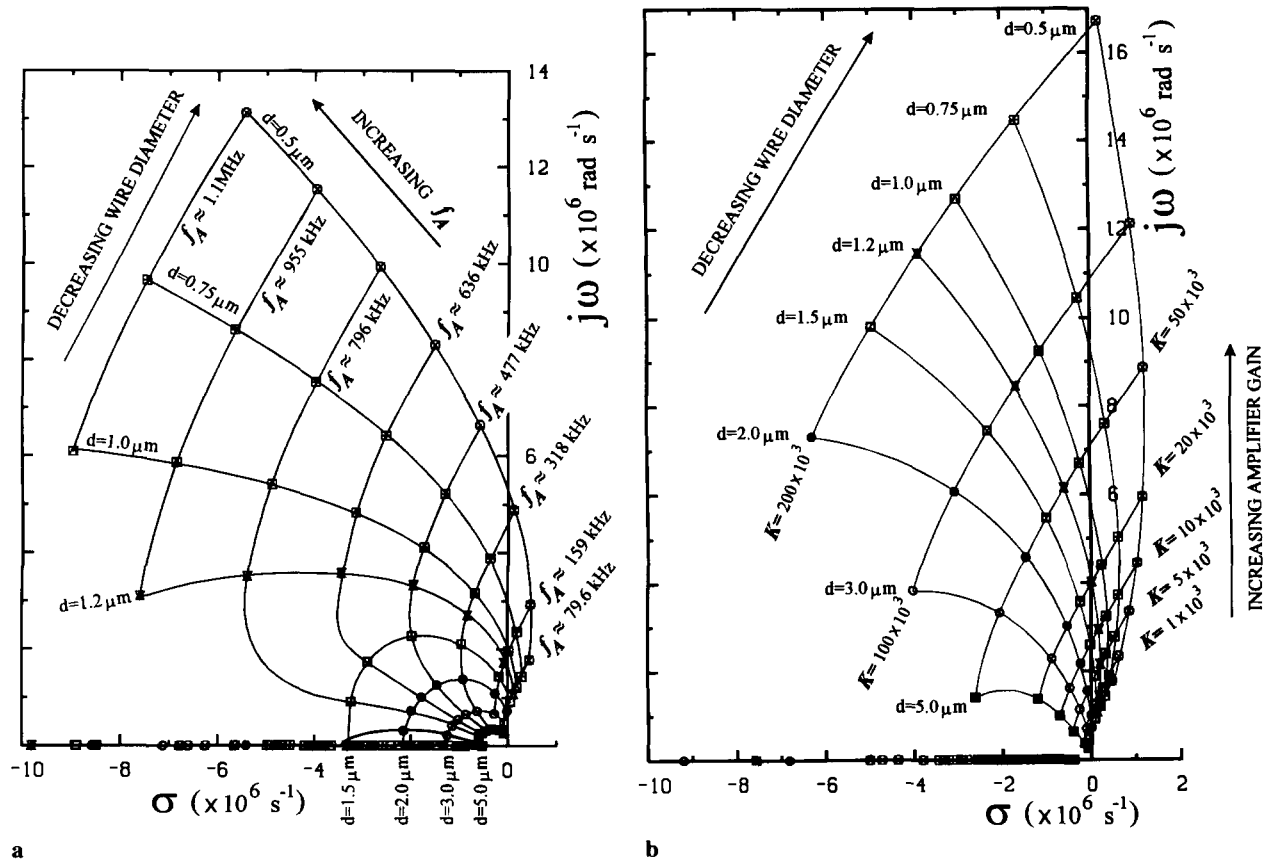


**Figure 11.** Calculated $s$-plane trajectories of the dominant poles for a range of wire diameters with the same length-to-diameter ratio. $R_b$ has been adjusted to closely give the same resistance ratio, that is, $R \approx 2$. $E_{qi} = 5$ mV, $L_b = 0.5$ $\mu$H, and $L_w = 0.1$ $\mu$H. Higher values of $K$ and $f_A$ are required for stability as the wire diameter is reduced. (*a*) Increasing $f_A$ (with constant gain $K = 1000$). (*b*) Increasing $K$ (with constant $f_A \approx 79.6$ kHz).

$\mathring{R}^2/R_w$ can be altered by adjusting the bridge resistors and the offset voltage. Finally, the frequency response of the feedback amplifier must be increased to obtain the same value of $M/T_w$.

If $f_A$ is fixed, then $M/T_w$ can be considerably larger with subminiature wires. This is especially significant because it has been demonstrated that the dominant poles become less damped as $f_A$ is reduced. If $f_A$ is too small, then the dominant poles may be unstable. Figure 11 shows the effect of reducing the wire diameter while maintaining the same length-to-diameter ratio (1:200) and the same resistance ratio $R \approx 2$ (by increasing $R_b$). At the lowest values of $f_A$ and $K$, the dominant poles are unstable for small wire diameters. As either $f_A$ or $K$ is increased, these poles move to the left half-plane and the systems become stable. The effect on the higher order poles is similar to the examples shown in Figs. 9 and 10.

The wire current required for a given resistance ratio is smaller for subminiature wires, so the static output voltage at the top of the bridge is considerably less than that obtained with conventional wires. Therefore, increasing $R_a$ and $R_c$ to obtain the same values of $R_a/R_w$ and $R_c/R_w$, as suggested above, would also help to restore the size of the output signal. However, this is not recommended because increasing $R_a$ and $R_c$ tends to reduce the damping of the dominant poles as shown in Fig. 12. The largest values of $R_a/R_w$ and $R_c/R_w$ correspond to the values used for the $d = 5.0$ $\mu$m wires in earlier sections. An even higher frequency response amplifier would be required to obtain a satisfactory system response under these conditions.

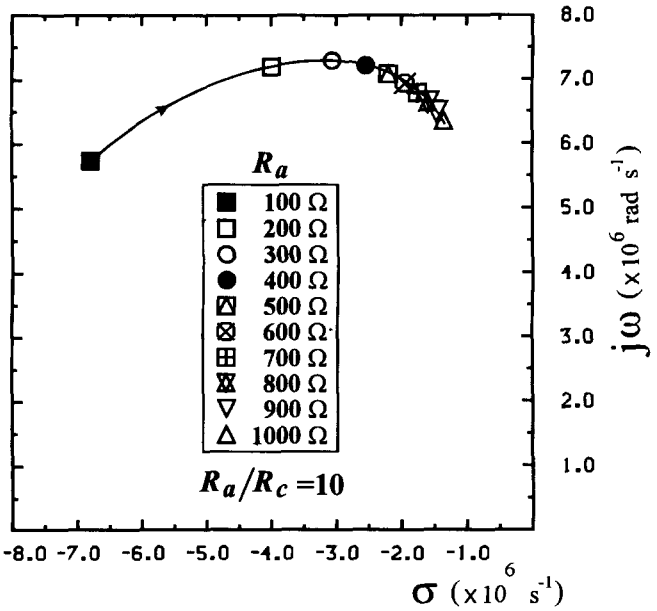


**Figure 12.** Increasing the upper bridge resistances $R_a$ and $R_c$ causes dominant poles to become less damped. Subminiature platinum filament of length 0.1 mm and diameter $d = 0.5$ $\mu$m ($R_g \approx 80$ ohms). Largest values of $R_a/R_w$ and $R_c/R_w$ are approximately the same as for the $d = 5$ $\mu$m wires in Figs. 4–11. $L_b = 8$ $\mu$H, $L_w = 1$ $\mu$H, $R_b = 1.6$ $k$ohm, and the amplifier frequency response $f_A \approx 1.6$ MHz, gain $K = 1000$, and offset voltage $E_{qi} = 5$ mV are constant. Air velocity is 20 m/s.

Insufficient frequency response of the feedback amplifier is the most likely cause of system instability when using subminiature wires.

## A PRACTICAL DESIGN

A new high-performance constant-temperature hot-wire anemometer has been built based on the ideas discussed in this paper. The first stage of the cascade is a high-performance instrumentation amplifier. The offset voltage is introduced into a buffer amplifier, which is followed by two variable gain stages. Two single-pole low-pass filters with variable roll-off frequency are located after the variable gain stages. Front panel access is provided for control of these parameters. The maximum large signal open-loop gain–bandwidth product of the feedback amplifier cascade has been measured in excess of $10^9$. The instrument also contains a square-wave generator for electronic tuning purposes as well as a "buck and gain" output amplifier, which is also fitted with a simple variable filter for conditioning the signals. In the standard configuration a tunable inductor is provided for cable compensation and the operating resistance is set via a thumbwheel switch. The anemometer may be optionally configured with a symmetrical bridge (i.e., $R_a = R_c$) and the thumbwheel switch and balance inductor removed from the bridge. The balance resistor $R_b$ is then located at the end of a length of coaxial cable that has been carefully chosen to match the probe cable. This configuration should offer superior compensation to the simple lumped inductor (by using an actual length of cable instead).

A detailed description of the design is given in [12]. Information such as fabrication drawings, parts list, specifications for a printed circuit board, and the companies responsible for fabrication and assembly are provided. Sufficient details are provided to enable the instrument to be constructed by others.

## PRACTICAL SIGNIFICANCE/USEFULNESS

The constant-temperature hot-wire anemometer is now used routinely in complex industrial flows such as the flow behind turbine blades, where stable high-frequency operation is essential. The information contained in this paper should act as a useful guide for achieving this objective. A flat frequency response is required in all flows to avoid biased data. The accuracy of measurements in a wide variety of flows will be increased if the undesirable modes of operation demonstrated in this paper are avoided.

## CONCLUSIONS

Doubts concerning the flatness of the frequency response will always remain until there is some direct experimental method for subjecting the instrument to accurately known velocity fluctuations over the operating frequency range. The primary source of the uncertainty lies in the behavior of the filament, which has not been considered here. It is well known that the filament cannot be considered to be a straight infinitely long circular cylinder with a uniform circumferential and spanwise surface temperature distribution. The behavior of a real filament is more complicated because heat waves propagate along its length. Thermal expansion cause it to develop a bow and to

behave like a buckled column. The bow deflects when loaded laterally, and the orientation appears to have an influence on the heat transfer coefficient of the filament. Perry [5] examined these and other aeroelastic and thermoelastic effects, which he proposed as being the source of the "ultimate uncertainty." However, other causes of deviation from the flatness of the frequency response can be identified, as shown in this paper, and these can be controlled if proper attention is given to the operation of the instrument.

The work described in this paper was performed over a period of several years. As mentioned in the introduction, the initial analysis was formulated while I was working at the Gas Dynamics Laboratory at Princeton University. The analysis was further developed while I was supported by the Center of Turbulence Research at Stanford University and by the MCAT Institute at NASA Ames Research Center. The design and development of the hardware was also supported by the Fluid Mechanics Laboratory Branch at NASA Ames Research Center.

## NOMENCLATURE

$A_j(s)$ polynomial for zeros for amplifier $j$, dimensionless

$B_j(s)$ polynomial for poles of amplifier $j$, dimensionless

$C_b$ balance capacitor, pF

$C_w$ lumped capacitor for modeling probe cable capacitance, pF

$c$ temperature coefficient of resistivity of wire, $K^{-1}$

$d$ diameter of wire filament, $\mu$m

$E_{o_n}$ dc output of $n$th amplifier, V

$E_{qi}$ dc component of offset voltage, V

$e_i$ small perturbation input voltage, V

$e_o$ small perturbation output voltage, V

$e_S$ small perturbation offset voltage, V

$e_w$ small perturbation voltage across wire arm of bridge, V

$e_{wire}$ small perturbation voltage across wire, V

$F_u(s)$ normalized frequency response of wire for velocity, dimensionless

$f_A$ frequency response of feedback amplifier, $s^{-1}$

$f_0$ frequency response of system, $s^{-1}$

$I_1, I_2$ dc bridge current, mA

$i_1, i_2$ bridge current fluctuations, mA

$K$ overall gain of feedback amplifier, dimensionless

$K_a$ gain of first equivalent amplifier, dimensionless

$K_b$ gain of second equivalent amplifier, dimensionless

$K_e$ gain of transfer function for offset voltage, dimensionless

$K_g$ thermal conductivity of fluid, W/(mK)

$K_u$ gain of transfer function for velocity, dimensionless

$L_b$ balance inductor, $\mu$H

$L_{b0}$ $L_b$ for ac balance [$= (R_c/R_a)L_w$], $\mu H$

$L_w$ lumped inductor for modeling probe cable inductance, $\mu$H

$l$ length of wire filament, $\mu$m

$M, M_1, M_2, M_3$ time constants of the feedback amplifier, s

Nu Nusselt number, dimensionless

$P(s)$ polynomial for system poles, dimensionless

$Q_e(s)$ polynomial for system zeros for offset voltage perturbations, dimensionless

$Q_u(s)$ polynomial for system zeros for velocity perturbations, dimensionless

$R$ resistance ratio ($= R_w/R_g$), dimensionless

$R_a, R_b, R_c$ resistive components of $Z_a(s)$, $Z_b(s)$, and $Z_c(s)$, ohms

$R_g$ cold resistance of wire, ohms

$R_w$ hot resistance of wire, ohms

$R_{wa}$ asymptotic value of $R_w$ as $E_{qi} \to 0$, *ohms*

$\mathring{R}$ bridge imbalance ($= R_w R_c - R_a R_b$) $ohm^2$

$S_u$ dc sensitivity to velocity fluctuations, V/(ms)

$s$ laplace variable ($= \sigma + j\omega$), $s^{-1}$

$T_w$ lumped time constant of hot wire, s

$U$ steady component of velocity, m/s

$u$ small perturbation velocity, m/s

$Z_a(s), Z_b(s), Z_c(s)$ bridge impedances, ohms

$Z_p(s)$ impendance in parallel with wire and $Z_s(s)$, ohms

$Z_s(s)$ impedance in series with wire, ohms

$Z_w(s)$ total impedance of wire arm of bridge, ohms

$Z_{wire}(s)$ impedance of wire, ohms

$Z_1(s), Z_2(s), Z_3(s)$ polynomials appearing in system transfer functions, dimensionless

### Greek Symbols

$\alpha$ $= R_w(R_w - R_g)/R_g$, dimensionless

$\sigma$ real component of $s$, $s^{-1}$

$\omega$ imaginary component of $s$, rad/s

$\zeta$ factor in damping of complex conjugate poles given by $Ts^s + 2\zeta Ts + 1$, dimensionless

## REFERENCES

1. Freymuth, P., and Fingerson, L. M., Electronic Testing of Frequency Response for Thermal Anemometers, *TSI Quart.* 3(4), 1977.
2. Perry, A. E., and Morrison, G. L., A Study of the Constant Temperature Hot-Wire Anemometer, *J. Fluid Mech.* **47**, 577–599, 1971.
3. Watmuff, J. H., Some Higher-Order Effects in the Behaviour of Constant Temperature Hot-Wire Anemometer Systems, ASME Symp. Thermal Anemometry, Cincinnati, OH, June 1987.

4. Smits, A. J., Perry, A. E., and Hoffman, P. H., The Response to Temperature Fluctuations of a Constant-Current Hot-Wire Anemometer, *J. Phys. E: Sci. Instr.* **11,** 909–914, 1978.
5. Perry, A. E., *Hot-Wire Anemometry,* Clarendon Press, Oxford, 1982.
6. Ossowski, X. X., Constant Temperature Operation of the Hot-Wire Anemometer at High Frequency, *Rev. Sci. Instr.* **19,** 881–889, 1948.
7. Davis, M. R., and Davies, P. O. A. L., The Physical Characteristics of Hot-Wire Anemometers, ISVR Tech. Rep. 2, Institute of Sound and Vibration, Southampton University, 1968.
8. Freymuth, P., Feedback Control Theory for Constant-Temperature Hot-Wire Anemometers, *Rev. Sci. Instr.* **38,** 677–681, 1967.
9. Wood, N. B., A Method for Determination and Control of the Frequency Response of the Constant-Temperature Hot-Wire Anemometer, *J. FLuid Mech.* **67,** 769–86, 1975.
10. Smits, A. J., and Perry, A. E., The Effect of Varying Resistance Ratio on the Behaviour of Constant-Temperature Hot-Wire Anemometers, *J. Phys. E: Sci. Instr.* **13,** 451–456, 1980.
11. Miller, I. S., Shah, D. A., and Antonia, R. A., A Constant Temperature Hot-Wire Anemometer, *J. Phys. E: Sci. Instr.* **20,** 311–314, 1987.
12. Watmuff, J. H., A High Performance Constant Temperature Hot-Wire Anemometer, NASA Contractor Rep. 177645, 1994.

Received August 8, 1994; revised December 16, 1994